



Wetting phenomena on micro-grooved aluminum surfaces and modeling of the critical droplet size

A.D. Sommers^{a,*}, A.M. Jacobi^b

^a Department of Mechanical and Manufacturing Engineering, Miami University, 56 Engineering Building, Oxford, OH 45056, USA

^b Department of Mechanical Science and Engineering, University of Illinois, 1206 West Green Street, Urbana, IL 61801, USA

ARTICLE INFO

Article history:

Received 27 June 2008

Accepted 6 September 2008

Available online 17 September 2008

Keywords:

Hydrophobic

Critical droplet

Condensate

Contact angle

Micro-grooves

Aluminum

ABSTRACT

The behavior of water droplets on aluminum surfaces with parallel grooves tens of microns in width and depth is considered, and a mechanistic model is developed for predicting the critical droplet size—droplets at incipient sliding due to gravity. The critical droplet size is nearly 50% smaller on micro-grooved surfaces than on the same surface without micro-grooves. The application of existing models fails to predict this behavior, and a new model based on empiricism is developed. The new model provides reasonable predictions of the critical droplet size for a given inclination angle, advancing contact angle, and maximum contact angle. When the grooves are aligned parallel to gravity, the maximum apparent contact angle does not occur at the advancing front but rather along the side of the droplet because of contact-line pinning. Droplets on these surfaces are elongated and possess a parallel-sided base contour shape. Novel data are provided for droplets in a Wenzel state, a Cassie–Baxter state, and combined state on micro-grooved surfaces, and the ability of the empirical model to handle these variations is explored. These findings may be important to a broad range of engineering applications.

© 2008 Elsevier Inc. All rights reserved.

1. Introduction

Understanding the behavior, shape, and size of the critical droplet is the key to understanding droplet retention on a surface. The so-called “critical droplet” [1] refers to a droplet of sufficient size so that the surface-tension retaining force is equal to the gravitational drainage force—that is, the critical droplet is at the point of incipient motion. Significant research has already been reported for critical droplets on smooth surfaces as well as homogeneously rough surfaces [2–5]. However, there is very little work in the open literature combining empirical data and modeling as a means for understanding water retention on micro-grooved surfaces. Our interest in water retention on such surfaces is motivated by recent advances allowing the inexpensive manufacture of aluminum fin stock with micro-grooves, and the potential for their use in heating, ventilation, air conditioning, and refrigeration (i.e. HVAC&R) systems, where managing water on the heat exchanger fins is a major design concern.

To achieve a truly water-repellent surface, the droplet contact line must be highly discontinuous and only possess metastable states of equilibrium. Extrand [6] argued that the two most important criteria for determining ultralyophobicity (i.e. the ability of a

surface to repel droplets independent of its contact angle) are contact line density and asperity height. Using a simple force analysis, Extrand developed expressions for the critical line density and critical asperity height for small droplets in terms of only the surface geometry, droplet volume, apparent advancing contact angle, and fluid properties, and then he tested these criteria using experimental data from various rough surfaces. Successful prediction of the collapse or suspension of droplets (wetting mode) was achieved. However, Extrand assumed spherical droplets, and the droplet volume supported by the pillars was neglected.

Using a mechanistic approach, Oliver et al. [7] showed that the Cassie–Baxter equation is valid for near-spherical mercury droplets on parallel-grooved nitrocellulose surfaces. However, for PPE droplets which were more cylindrical, the Cassie–Baxter equation was not valid, and Oliver et al. developed a new expression from a two-dimensional force balance that approximates the apparent contact angle.

Morita et al. [8] offered insight into the anisotropic wetting behavior of micro-patterned, two-component fluoroalkylsilane monolayer surfaces with alternating hydrophilic/hydrophobic lines of width 1–20 μm . For all line widths, they observed that the static and dynamic contact angles of droplets oriented orthogonally to the stripes were 10–30° larger than those of droplets oriented parallel to the stripes. Sliding angle data also showed lower tilt angles for droplets sliding parallel to the stripes than for droplets sliding orthogonally to the stripes. However, no general model explain-

* Corresponding author. Fax: +1 (513) 529 0717.

E-mail address: sommerad@muohio.edu (A.D. Sommers).

Nomenclature

Bo	Bond number, $\rho g D^2 \sin \alpha / \gamma$	θ	apparent contact angle
D	equivalent diameter, $2(Lw)^{1/2}$	λ	retentive force correction term
D_c	critical diameter, $2L$	ρ	liquid density
F	force	ϕ	azimuthal angle
g	acceleration of gravity	<i>Subscripts and superscripts</i>	
L	half-length of a droplet; major radius	1	contact angle at $\phi = 0^\circ$
S	circumferential arc length	2	contact angle at $\phi = 180^\circ$
w	half-width of droplet; minor radius; micro-groove width	adv	advancing
<i>Greek symbols</i>		eq	equivalent
α	surface inclination angle	g	gravitational
β	droplet aspect ratio, L/w	max	maximum
γ	surface tension of liquid–vapor interface	min	minimum
δ	micro-groove depth	PS	parallel-sided
ζ	base contour radius	rec	receding
		s	relating to surface tension

ing how the contact angle varied with the azimuthal angle was offered.

Yoshimitsu et al. [9] studied the sliding behavior and contact angle variation of water droplets on hydrophobic pillar and groove structures prepared from a silicon wafer by dicing it and then coating it with fluoroalkylsilane. Although the contact angle was higher on the pillar structure, the groove structure exhibited better water-shedding characteristics in the parallel direction than the pillar structure because of its low energy barrier to the movement of the contact line.

In perhaps the study most germane to the present work, Chen et al. [10] examined the apparent contact angle and shape of water droplets on parallel-grooved surfaces from both a numerical and experimental perspective. In both cases, the apparent contact angle viewed from the front (line of sight parallel to grooves and gravity) was typically larger than the contact angle viewed from the side, an observation that Chen and co-workers attributed to the pinning of the droplet against the pillars. They also noted that a cubic equation better fit the base contour of the drop than an ellipse, because it was “flatter” on the sides. In their model, however, droplet volume, base contour shape, and contact angle are all needed *a priori* to determine the equilibrium droplet shape. Chen and co-workers also examined very small water droplets (i.e. 0.59–5.7 μL) and did not quantify the relationship between the contact angle and the azimuthal angle, nor was information about critical inclination angle or maximum droplet size provided.

Extrand and Kumagai [11] studied water and ethylene glycol droplets at the critical condition on polymer and silicon surfaces using a tilt table with an emphasis on contact angle hysteresis, droplet shape, and the retentive force. They found that those surfaces with the largest contact angle hysteresis also produced the most elongated drops. For these experiments, however, the base contour was taken as elliptical, and $\cos \theta$ was assumed to vary linearly around the base of the drop.

In a numerical study of droplets at the critical condition, Dimitrakopoulos and Higdon [12] solved for the droplet configuration that produced minimum contact angle hysteresis (i.e. $\theta_A - \theta_R$) for a specified advancing angle θ_A and Bond number. The result, however, produced a nearly step-wise variation of the contact angle from θ_A to θ_R around the base of the drop.

In two recent reports by El Sherbini and Jacobi [13,14], the droplet shape was approximated using a method that fits the droplet profile with two circles sharing a common tangent at the apex of the droplet. With experimentally determined base contours and contact angle variation, this method was found to allow ac-

curate calculations of the drop volume. This work, however, was intended only for regular surfaces of homogeneous roughness. The azimuthal variation of the contact angle around the base of the drop was found to follow a third-order polynomial, an observation that differs from the present study as will be shown later. Furthermore, in this earlier work, the base contour was taken to be elliptical, and the contact line was assumed to be continuous. These conditions may not prevail on heterogeneously rough surfaces with micro-grooves. In another recent work, Bouteau et al. [15] showed that an elongated, parallel-sided droplet shape provided a better fit with experimental data and cited the importance of the capillary forces at the front and rear edges of the droplet. However, this work was performed on ideal Langmuir–Blodgett surfaces, and the data did not compare well with the model predictions of [13,14].

Most attempts to radically change surface wettability have focused not only on surface geometry (the focus of this research) but also on modification of the surface free energy by chemical treatment. This dualistic approach is not only more costly but perhaps more restrictive in industrial applications where thermal cycling and fouling raise legitimate concerns over coating robustness.

The overall objective of this work was to measure and model the retention of water droplets on micro-grooved aluminum surfaces. We reported a dry-etching technique to create such surfaces earlier (Sommers and Jacobi [16]), and adopted that method in this work because it permits excellent control of the surface geometry. We note that scalable paths to mass production of such surfaces exist. In this study, droplets in the range of 5 to 25 μL were injected onto the surface using a precision micro-syringe and then photographed using a KAPPA DX 10-1394a high-resolution CCD camera typically within 2 min of deposition. Recent work has shown that the retention force may be a function of time so the ability to photograph the droplet in a quick and consistent manner is important [17]. According to Yadav et al. [18], the error in the measured advancing and receding contact angles due to this droplet resting time would be less than $\pm 0.4^\circ$ and 0.6° , respectively, which is within the experimental uncertainty of this work. The camera was mounted opposite to a light source on an arm that could be rotated around a fixed plate containing the test surface and droplet. The sample and water droplet were placed inside a vapor-tight, transparent box to minimize the effect of evaporation on droplet geometry during image acquisition. Determination of the critical inclination angle for sliding on these surfaces was accomplished using a tilt-table assembly. Standard image analysis software was used to process the images and determine the contact angle and base dimensions of the droplet. Multiple mea-

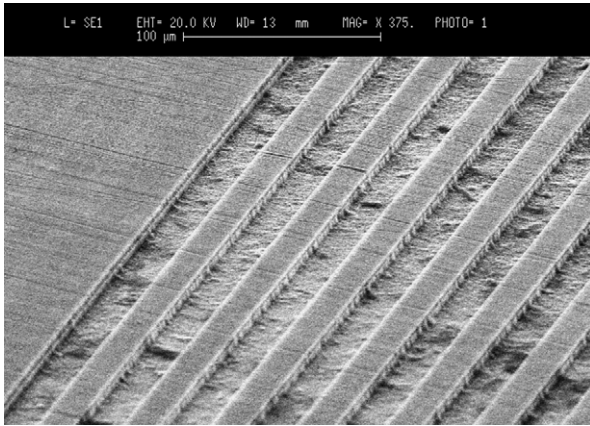


Fig. 1. SEM image of sample 6 (magnification = 375 \times) after reactive ion etching.

Table 1
List of manufactured micro-grooved surfaces.

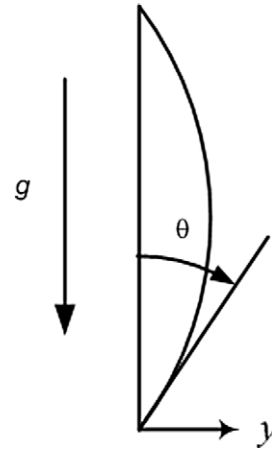
Sample No.	Pillar width, w (μm)	Pillar depth, δ (μm)	Ratio w/δ
Baseline	–	–	–
1	26.8	5.2	0.194
2	25.2	15.7	0.623
3	23.2	27.0	1.174
4	14.0	6.19	0.442
5	10.4	22.0 ^a	1.964
6	4.62	6.89	1.490
7	19.9	6.89	0.346
8	24.9	6.89	0.277
9	38.0	6.89	0.181
10	15.6	26.7	1.455
11	19.6	26.7	1.158
12	35.3	26.7	0.643

^a Indirect measurement.

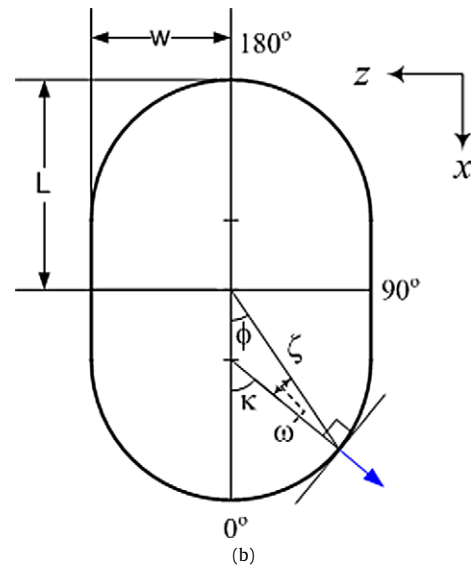
measurements were recorded for each droplet volume which permitted the critical inclination angle and related droplet diameter to be checked for consistency. The maximum uncertainty in the measured contact angle was approximately 3 $^\circ$ while the uncertainty in the critical inclination angle was only 1 $^\circ$. Typical uncertainty in drop diameter was 2–3% with the maximum uncertainty not exceeding 7%. Aluminum was chosen because it is naturally hydrophilic and is the material of choice in many heat and mass transfer applications. The groove geometry was chosen (over more complex designs such as posts) because it is simple, may be more robust than posts, and because it would be easier to micro-emboss in mass production. A SEM image of a sample surface ($w = 4.6 \mu\text{m}$, $\delta = 6.9 \mu\text{m}$) is shown in Fig. 1. Geometric data for all produced specimens are provided in Table 1.

2. Critical droplets

The so-called critical droplet refers to a droplet large enough that the surface tension retaining force is equal to the gravitational drainage—such a drop is at the point of incipient motion. Understanding the shape and size of the critical droplet is the key to understanding the mechanisms of droplet retention on a surface. Perhaps more importantly, being able to accurately predict the critical droplet size for sliding on a given surface of given inclination is essential to knowing the amount of water that will be retained on that surface. Therefore, models which can predict critical droplet characteristics represent important design tools and are useful in applications where simultaneous heat and mass transfer occur. In order to predict the critical droplet volume, V , on a surface inclined at an angle α from horizontal, consider a force balance in



(a)



(b)

Fig. 2. Coordinate system and geometric description of an elongated droplet.

the x -direction (see Fig. 2). The x -component of the gravitational force is

$$F_{gx} = \rho g V \sin \alpha, \quad (1)$$

and for the case shown in Fig. 2, the surface tension retaining force in the x -direction is

$$F_{sx} = -2\gamma \int_0^\pi \zeta \cos \theta \cos(\phi + \omega) d\phi, \quad (2)$$

which is similar to the expression used by Extrand and Kumagai [11]. In Eq. (2), ζ is the distance from the droplet center to the contact line (local radius), θ is the apparent contact angle, and ϕ is the azimuthal angle which is the angle formed with respect to a line parallel to the direction of the grooves. As can be seen in Fig. 2, the $\cos(\theta)$ term projects the force into the x - z plane, and the $\cos(\phi + \omega)$ term projects it into the x -direction; the inclusion of ω can be important for non-circular droplets with large elongations (as will later be shown to form on micro-grooved surfaces). More specifically, the angle $(\phi + \omega)$ is necessary to maintain orthogonality between the surface tension force and the contact line along the curved portion of the droplet base contour. Mathematically, ω is found using the law of cosines for the curved portion of the droplet base contour such that

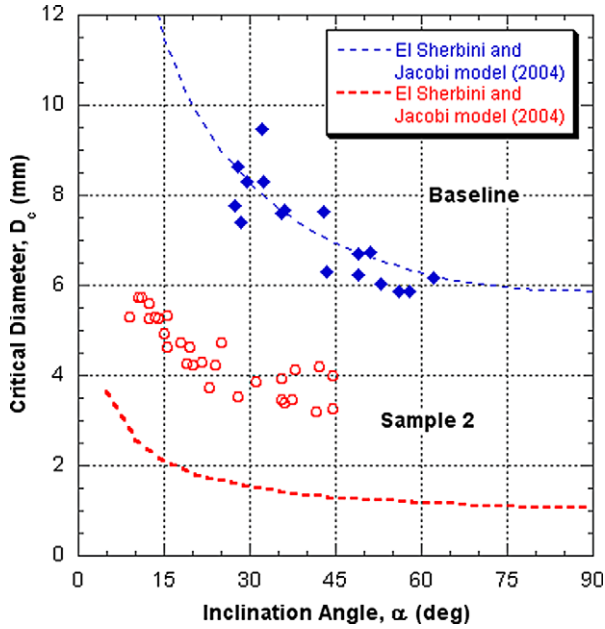


Fig. 3. Critical droplet diameter on baseline and micro-grooved surface and comparison to existing model. The droplet size at incipient sliding was reduced by approximately 50% for the micro-grooved surface, and the existing model failed to predict this behavior.

$$\cos \omega = \left(\frac{1}{2w\zeta} \right) (w^2 + \zeta^2 - (L - w)^2), \quad (3)$$

whereas for the parallel-sided portion of the droplet bounded by $\phi < 90^\circ$, ω is set equal to 90° minus ϕ (i.e. ω is very small). Closure of the force balance requires a description of how the local radius and contact angle vary with the azimuthal angle, $\zeta(\phi)$ and $\theta(\phi)$, and a method for calculating the droplet volume accurately. For droplets on a “flat” surface, El Sherbini and Jacobi [13,14] provided such closure by fitting experimental data, estimating droplet shape with the two-circle method, and then demonstrating that the model worked well for a range of fluids and surfaces.

Early data from our laboratory demonstrated that the critical droplet size for sliding on the micro-grooved samples was reduced as compared to the baseline specimen; furthermore, the existing model failed to accurately predict this behavior. To demonstrate this, the critical droplet diameter is plotted in Fig. 3 for both the baseline specimen and sample 2 ($\delta = 15.7 \mu\text{m}$) and compared to this existing force balance model [13,14]. Good agreement was achieved between the model and the baseline data; however, the existing model clearly failed to predict the critical droplet size on the micro-grooved surface. Because there was nothing to suggest that the force-balance approach itself had somehow been vitiated on these micro-grooved surfaces, this finding implied failure of the assumed contact angle variation, base contour shape, drop shape (and potentially other tacit assumptions).

The results shown in Fig. 3 prompted efforts to extend and refine the model to make it appropriate for micro-grooved surfaces. A robust and well-tested model to predict the critical droplet size for sliding on a micro-grooved surface could serve as a design tool and provide insight into the retention mechanisms. In order to extend the existing force-balance model for flat surfaces to micro-grooved surfaces, the empirical bases for $\zeta(\phi)$ and $\theta(\phi)$ were re-examined. Moreover, the tacit assumption of a continuous solid–liquid–gas contact line was re-examined. Following prior work [13,14], reformulation of the force balance model was pursued by casting base contour shape in terms of droplet elongation (aspect ratio), and the variation of the contact angle was scaled with contact angle hysteresis. As will be elaborated later, this ap-

proach recognizes the relevant physics. The potential for contact-line discontinuity required a completely new approach, because such discontinuity is not manifest on flat surfaces.

2.1. Azimuthal contact angle variation on micro-grooved surfaces

For conventional surfaces such as the baseline surface, the fit of Eq. (4) has been shown to work well:

$$\cos \theta = 2 \frac{\cos \theta_{\max} - \cos \theta_{\min}}{\pi^3} \phi^3 - 3 \frac{\cos \theta_{\max} - \cos \theta_{\min}}{\pi^2} \phi^2 + \cos \theta_{\max}, \quad (4)$$

where θ_{\max} refers to the apparent contact angle at $\phi = 0^\circ$ and θ_{\min} refers to the apparent contact angle at $\phi = 180^\circ$ [13]. However, for the micro-grooved surfaces, Eq. (4) was found to poorly represent the data. Because on the micro-grooved surfaces the contact line is ‘pinned’ on the sides of the drop, the micro-grooves confine the droplet on the surface and impede spreading in the direction perpendicular to the grooves. Thus the channels serve as periodic energy barriers to droplet spreading and cause the maximum apparent contact angle to occur at $\phi = 90^\circ$ instead of at $\phi = 0^\circ$. This interesting phenomenon (shown in Fig. 4) was observed at various angles of surface inclination as well as for various droplet volumes. Therefore, a new model was developed to predict this unusual behavior of the contact angle; after some trial and error, the following form was adopted:

$$\cos \theta = C_1 \cos^3 \phi + C_2 \cos^2 \phi + C_3 \cos \phi + C_4. \quad (5)$$

In order to force the equation to capture the behavior discussed above, it was subjected to the following constraints:

$$\cos \theta|_{\phi=0} = \cos \theta_{\text{adv}}, \quad (6)$$

$$\cos \theta|_{\phi=\frac{\pi}{2}} = \cos \theta_{\max}, \quad (7)$$

$$\cos \theta|_{\phi=\pi} = \cos \theta_{\text{rec}}, \quad (8)$$

and

$$\left. \frac{d(\cos \theta)}{d\phi} \right|_{\phi=0} = \left. \frac{d(\cos \theta)}{d\phi} \right|_{\phi=\frac{\pi}{2}} = \left. \frac{d(\cos \theta)}{d\phi} \right|_{\phi=\pi} = 0, \quad (9)$$

where θ_{adv} and θ_{rec} were measured on the inclined surface. The resulting model which predicts the contact angle on these micro-grooved surfaces is

$$\cos \theta = \left(\frac{\cos \theta_{\text{adv}} - \cos \theta_{\text{rec}}}{2} \right) \cos^3 \phi + \left(\frac{\cos \theta_{\text{adv}} + \cos \theta_{\text{rec}} - 2 \cos \theta_{\max}}{2} \right) \cos^2 \phi + \cos \theta_{\max}, \quad (10)$$

where, in this definition, θ_{\max} refers to the apparent contact angle at $\phi = 90^\circ$.

Shown in Fig. 4 are contact angle data collected on sample 2 for various droplet volumes at various angles of surface inclination. In Fig. 4a, the azimuthal variation of the contact angle is shown for a 10- μL injected water droplet at an inclination angle of 90° . The maximum observed contact angle for this droplet occurred at a location along the side of the droplet (i.e. $\phi = 90^\circ$) and was approximately 133° . In contrast, the contact angle observed at the advancing front was only 96° . Also shown in these figures is the newly developed model for azimuthal contact angle variation which yielded favorable agreement with the collected data.

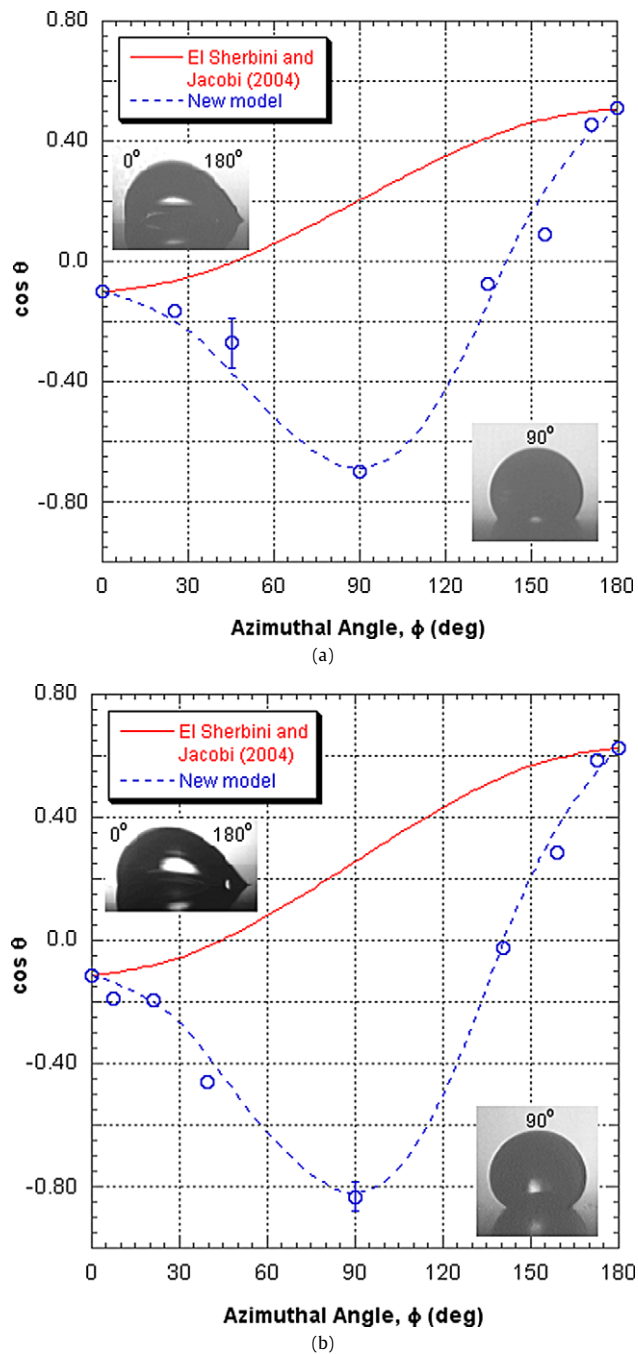


Fig. 4. Azimuthal contact angle variation for (a) 10 μL droplet, $\alpha = 90^\circ$ on sample 2, and (b) 15 μL droplet, $\alpha = 60^\circ$ on sample 2.

2.2. Droplet aspect ratio on micro-grooved surfaces

The aspect ratio was determined by measuring the major and minor axes of the droplet base at $\phi = 0^\circ$ and $\phi = 90^\circ$. Because the apparent contact angle was sometimes greater than 90° , side profile images of the droplet were used in lieu of frontal images. As shown in Fig. 5, the presence of micro-grooves on the surface tends to elongate the droplet even for very small inclination angles (i.e. $Bo \rightarrow 0$). It was also found that droplets on these surfaces were slightly more elongated than those on flat surfaces [13,14]. This might be expected because the channels impose a preferential direction for spreading. A least-squared-error regression was performed as a function of both the channel geometry and Bond number when operating in this mode. The inclusion of the Bond

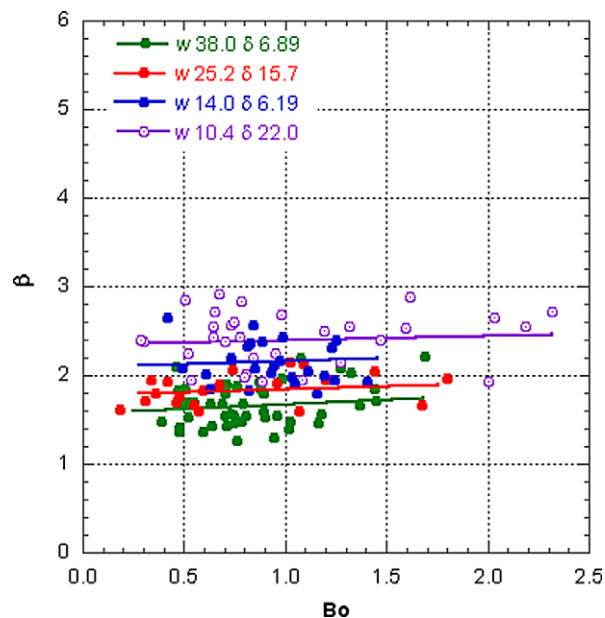


Fig. 5. The aspect ratio data reveal that these droplets are elongated even at low angles of inclination.

number follows prior work [13,14] and recognizes the competition between potential and surface energy relevant to elongation; the inclusion of channel geometry recognizes surface energy differences associated with liquid–vapor versus liquid–solid interfaces. The functional form was selected through trial and error and has no apparent physical significance.¹ The resulting expression for droplets that do not (or, nearly do not) wet the grooves is

$$\beta = 1.0 + 0.096Bo + 1.02Bo^{0.081} \left(\frac{\delta}{w} \right)^{0.297} \quad (11)$$

It should also be pointed out that this correlation was constructed so that as groove depth vanishes (i.e. $\delta \rightarrow 0$) it will collapse to $\beta = 1.0 + 0.096Bo$, which was shown to be suitable for flat surfaces in an earlier work [13,14]. The fit was based on a sample size of $n = 125$. For 70% of the data, the experimental measurement was within 15% of that given by Eq. (11); while for 85% of the data, the difference was within 20%. The average error between the correlation and the data was 12.3% with the maximum error not exceeding 32%.

2.3. Minimum contact angle ratio on micro-grooved surfaces

Contact angle hysteresis is captured using the ratio of the minimum contact angle to the advancing contact angle. The contact angles were determined by averaging at least four separate measurements for each droplet. The data are plotted in Fig. 6, along with a curve providing a reasonable fit to these data ($r^2 = 0.84$):

$$\frac{\theta_{\min}}{\theta_{\text{adv}}} = -0.260Bo + 0.808. \quad (12)$$

The form of Eq. (12) follows that of earlier work for flat surfaces [13,14]. The figure provides the variation of $\theta_{\min}/\theta_{\text{adv}}$ with the Bond number for both composite droplets and wetting droplets on five different micro-grooved surfaces. The minimum angle θ_{\min} is observed to decrease with increasing Bond number meaning the

¹ The authors recognize that for flat surfaces the fact that a least-squared-error fit to a large data set yields a linear relationship very close to $\beta = 1 + Bo/10$ is suggestive of some physical significance.

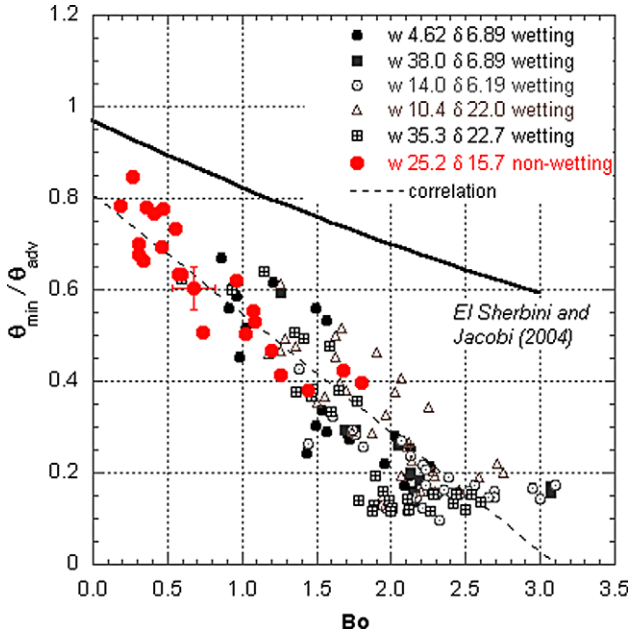


Fig. 6. The minimum contact angle ratio varied linearly with the Bond number and followed approximately the same relationship for all examined surfaces.

minimum contact angle decreases with increasing inclination angle and/or increasing droplet diameter. Because droplets on these surfaces are more elongated than on flat surfaces, the droplet diameters are larger, and the $\theta_{\min}/\theta_{\text{adv}}$ ratio decreases more rapidly with Bond number than it does for the conventional surface (the fit to data for a flat surface is given in Fig. 6). Other researchers have also observed this linear relationship between the minimum contact angle and the Bond number. The numerical work of Milinazzo and Shinbrot [4] is one such example. Although it is not altogether obvious, it is interesting that the behavior of the $\theta_{\min}/\theta_{\text{adv}}$ ratio is approximately the same for all five of the surfaces that were examined. It should also be emphasized that although the correlation intercepts the ordinate axis at approximately 0.80, it is known that θ_{\min} should equal θ_{adv} for the case of zero inclination (i.e. $Bo = 0$). However, because it agreed well with the data in the range $0.3 < Bo < 2.5$, the correlation was retained in its original form. Finally, it is important to note here that the contact angle used in defining this ratio is the advancing contact angle and not the maximum contact angle to be consistent with earlier correlations.

2.4. Droplet base contour shape on micro-grooved surfaces

In view of the larger elongation observed for droplets on micro-grooved surfaces, it is not surprising that a revised description of the droplet base contour is needed. The base contour shape and contact angle variation are both important to determining surface ultralyophobicity. When modeling the shape of water droplets, prior research has often adopted an elliptical (or even circular) base contour shape [3,4,11]. Although this choice proves adequate for droplets on conventional surfaces, the larger elongation on micro-grooved surfaces calls such a choice into question. Three possible base-contour shapes were considered in detail. Following the work of Chen et al. [10], who used a cubic equation for droplets on surfaces with parallel grooves, two cubic base contours were considered and compared to the elliptical form. One cubic form was obtained by starting with

$$\zeta(\phi) = a_1\phi^3 + a_2\phi^2 + a_3\phi + a_4, \quad (13)$$

which, when subjected to the following geometrical constraints,

$$\zeta|_{\phi=0} = L \quad \text{and} \quad \zeta|_{\phi=\pi/2} = w, \quad (14)$$

with

$$\left. \frac{d\zeta}{d\phi} \right|_{\phi=0} = 0 \quad \text{and} \quad \left. \frac{d\zeta}{d\phi} \right|_{\phi=\pi/2} = 0, \quad (15)$$

yields

$$\zeta(\phi) = \frac{16}{\pi^3} \left(\frac{L\beta - L}{\beta} \right) \phi^3 - \frac{12}{\pi^2} \left(\frac{L\beta - L}{\beta} \right) \phi^2 + L. \quad (16)$$

In Eq. (16), ζ is the base radius, which is a function of the azimuthal angle, ϕ . The second cubic shape considered was that of Chen et al. [10], which can be re-written as

$$\zeta(\phi) = \left[\left(\frac{|\cos \phi|}{L} \right)^3 + \left(\frac{\beta|\sin \phi|}{L} \right)^3 \right]^{-1/3}. \quad (17)$$

Finally, the elliptical form was also considered:

$$\zeta(\phi) = \frac{L}{\sqrt{\cos^2 \phi + \beta^2 \sin^2 \phi}}. \quad (18)$$

In exploring the suitability of these three base-contour shapes for droplets on micro-grooved surfaces, the elliptical shape was found to be inadequate, failing to represent the parallel-side shape of the elongated droplets. The cubic form given by Eq. (16) is not truly parallel-sided; nonetheless, it is ‘flatter’ than an ellipse and provides a more realistic representation of the actual shape. However, for droplets with $\beta \geq 2$, which can form on micro-grooved surfaces (cf. Fig. 5), the shape given by Eq. (16) manifests an anomalous side curvature producing a “bone-shaped” droplet. For this reason, the cubic form of Chen et al. [10] (Eq. (17)) was chosen to represent the base contour shape of droplets on the micro-grooved surface. A comparison of all three candidate base-contour shapes and an application of Eq. (17) to the base contour of a typical droplet is provided in Fig. 7. The ability of the model to capture both the droplet dimensions and degree of elongation is clearly demonstrated in the figure.

2.5. Contact line discontinuity

For composite droplets, the micro-grooves create discontinuities in the three-phase contact line. These discontinuities occur when air becomes trapped underneath the water droplet, and the droplet ceases to fill the micro-grooves [9,10]. In order to account for these contact line discontinuities, an additional corrective term λ was added to the equation for finding the surface tension force. To a first approximation,

$$F_{sx} = -2\gamma\lambda \int_0^\pi \zeta \cos \theta \cos(\phi + \omega) d\phi, \quad (19)$$

where

$$\lambda = \frac{4 \int_0^{\pi/2} \zeta_{\text{actual}} d\phi}{4 \int_0^{\pi/2} \zeta_{\text{apparent}} d\phi} \quad (20)$$

and the integration involving ζ_{actual} yields the portion of the droplet perimeter in contact with the surface, and the integration involving ζ_{apparent} yields the entire droplet perimeter. It is important to note that λ is not an independent “tuning” parameter. Rather, it depends directly upon the channel geometry, base contour shape, and wetting mode and represents the fraction of the perimeter of the discontinuous droplet shape over the perimeter of the continuous droplet shape. Practically, λ is found by summing together the individual wetted arc lengths of the discontinuous

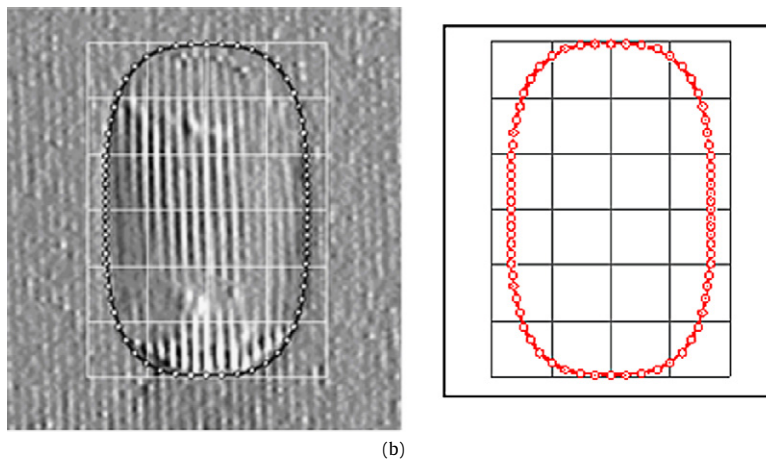
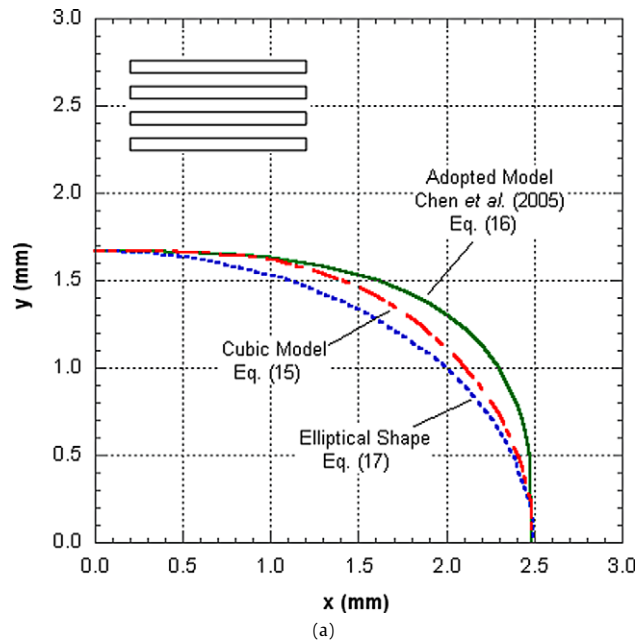


Fig. 7. A comparison of different base contour shapes: (a) candidate base-contour shapes for a droplet where $L = 2.5$ mm and $\beta = 1.5$, and (b) application of Eq. (16) to a typical condensed droplet with $\beta = 1.68$.

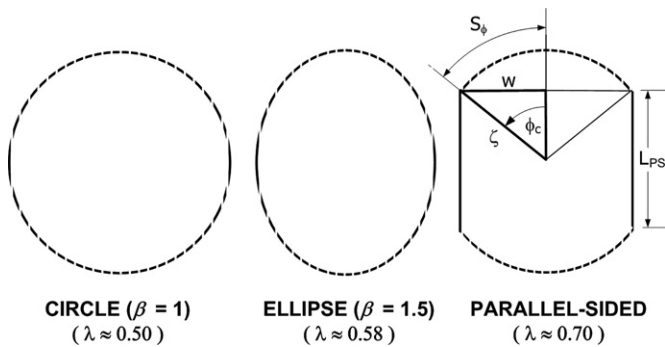


Fig. 8. Typical λ values for different base contour shapes when the droplet does not wet the surface.

three-phase contact line and dividing this quantity by the droplet perimeter if a continuous contact line were assumed. For example, in the case of a circular contact line, the value of λ would be approximately 0.5 for a non-wetting droplet on a micro-grooved surface of equal channel spacing. This value increases slightly for an elliptical contour due to the presence of longer continuous arc length segments on the sides of the droplet and is still larger for the parallel-sided droplet as shown below in Fig. 8. Tabulated val-

Table 2
Calculated values of λ for critical composite droplets.

Inclination angle, α		w/δ	w/δ	w/δ
		25.2/15.7	10.4/22.0	15.6/22.7
20°	λ (PS)	0.67	0.66	0.66
	λ (ES)	0.54	0.53	0.53
40°	λ (PS)	0.70	0.68	0.68
	λ (ES)	0.56	0.55	0.54
60°	λ (PS)	0.71	0.69	0.69
	λ (ES)	0.57	0.55	0.55
80°	λ (PS)	0.71	0.70	0.69
	λ (ES)	0.57	0.56	0.55

Note: PS = parallel-sided shape, ES = elliptical shape.

ues for a few of these surfaces are given in Table 2. As shown in this table, composite droplets on these surfaces at the onset of sliding typically had λ values that varied between 0.65 and 0.75. By comparison, if an elliptical base contour had been used, these λ values would have been smaller and would have varied between 0.53 and 0.58, which would result in an under prediction of the surface-tension force.

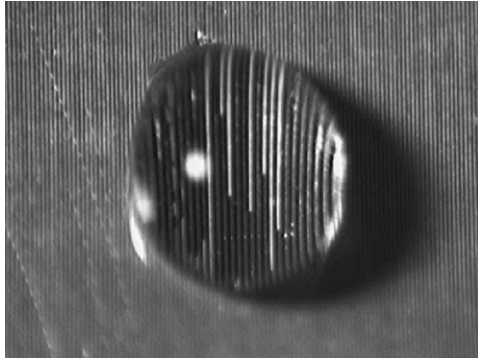


Fig. 9. This representative image taken immediately following droplet deposition shows that the droplet is only partially non-wetting.

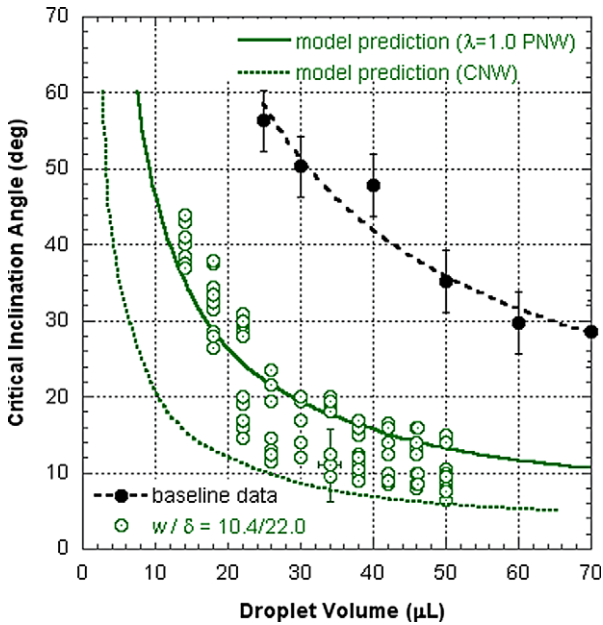


Fig. 10. Experimental data and model prediction for sample 5.

In some cases, droplets were neither fully wetting nor truly non-wetting. An example is provided in Fig. 9, where a droplet placed on sample 2 is in a partially non-wetted state. Some channels are wetted, some partially wetted, and some are completely non-wetted. As a consequence, a more complex contact line is formed than is considered in putting forward Eqs. (19) and (20), which assume a perfectly non-wetting case. Thus, the calculated λ value will always be lower than what is physically realized for these surfaces which exhibit partially non-wetting droplets. Imperfect suspension of the droplet creates a contact line that is longer and more complex than the modeled geometry, in which the contact line is confined to the base contour, and this complexity results in an under prediction of the surface-tension force.

3. Model predictions

Using the fits to data for critical droplets described in the prior section, the force-balance model was applied. In addition to fluid properties, the model requires as inputs the surface inclination angle (α), advancing contact angle (θ_{adv}), contact angle at $\phi = 90^\circ$ (θ_{max}), and channel geometry (δ, w). Because at incipient motion $\theta_{min} = \theta_{rec}$, Eq. (12) allows the receding contact angle to be calculated for a given Bond number. Equation (10) then provides the contact angle variation along the base contour. The elongation is determined by Eq. (11) for a given Bond number, which

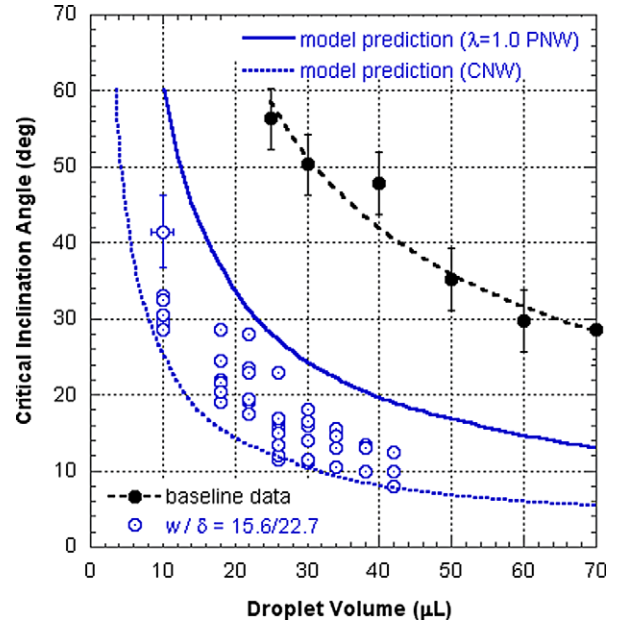


Fig. 11. Experimental data and model prediction for sample 10.

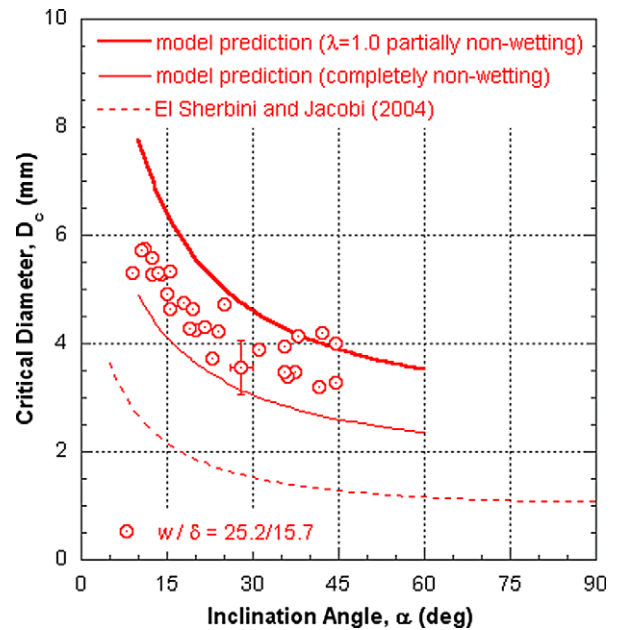


Fig. 12. Experimental data and model prediction for sample 2.

is then used with Eq. (17) to obtain the base contour shape. Thus, the model can be implemented by guessing a droplet diameter, calculating the Bond number, determining contact angle variation and base contour shape, then calculating droplet volume using the two-circle method of El Sherbini and Jacobi [13,14]. Once the volume is calculated, the force balance is implemented using Eq. (1) and Eqs. (19), (20) for a specified wetting condition (Cassie–Baxter or Wenzel). Iteration of droplet size is required until force balance equality is achieved.

Representative results of applying this model to a few of the surfaces experiencing the Cassie–Baxter mode of wetting are shown below in Figs. 10–12. The critical inclination data were collected by placing droplets of different volumes on the surface and then slowly tilting the surface until the point of incipient droplet motion. An example of a 30 μL droplet on sample 5 at the onset of sliding is shown in Fig. 13. In Figs. 10–12, two different model

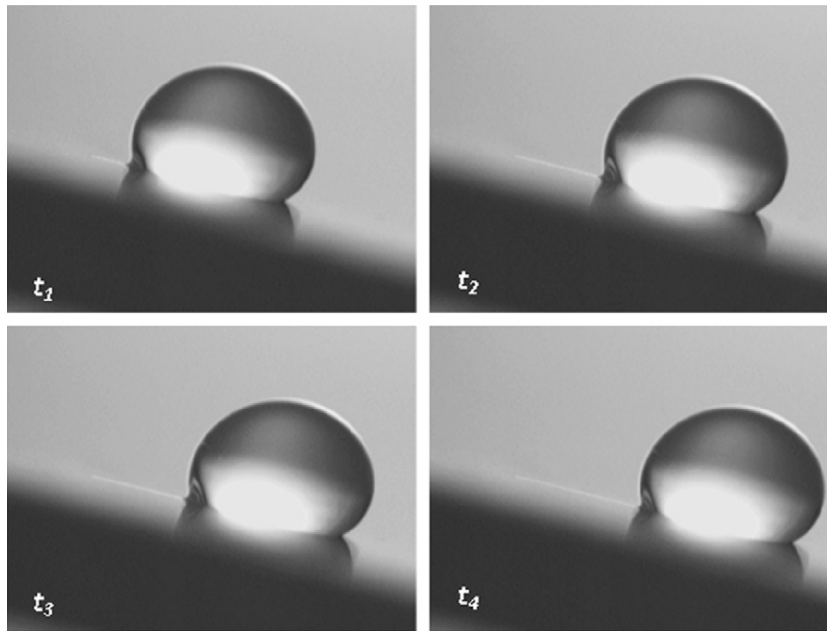


Fig. 13. Images of a critical composite droplet on sample 5. At $t = t_1$, the droplet is stationary; at subsequent (arbitrary) times, t_2, t_3, t_4 , the droplet is slowly sliding down the inclined surface.

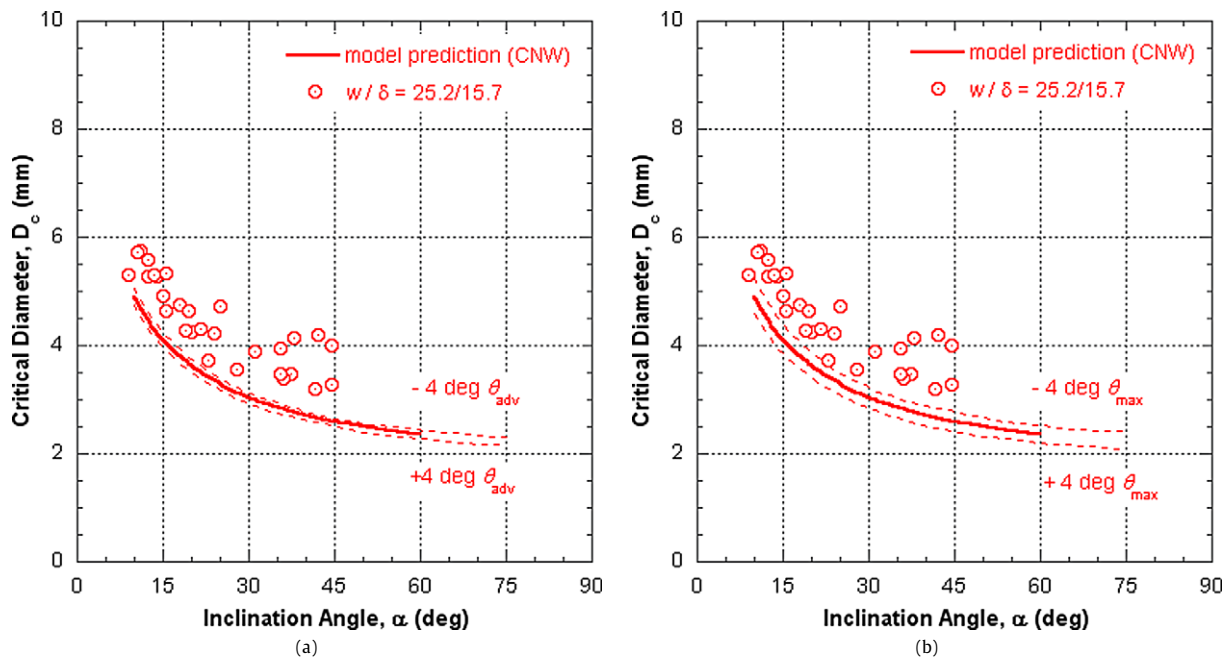


Fig. 14. Sensitivity analysis results for the new mechanistic model of droplet retention that shows both (a) the effect of modifying θ_{adv} , and (b) the effect of modifying θ_{max} .

prediction curves are shown. One is the completely non-wetting (CNW) case which uses the definition for λ shown in Eq. (20) to handle the surface contact-line discontinuities (values shown in Table 2). As a result, this prediction represents the ideal case where the droplet is assumed to not wet any of the micro-grooves and rests completely on top of the pillars—an assumption already shown to not be entirely true. In the second model prediction, a λ (somewhat arbitrary) value of 1.0 is used to depict the partial non-wetting (PNW) case where the surface wetting and non-wetting effects perfectly negate each other. This treatment is equivalent to the removal of λ from Eq. (19). As a result, these model predictions represent the boundaries of non-wetting. Despite the scatter present in the data, the wetting models capture the overall trends associated with surface non-wetting behavior quite well. In fact,

the two wetting models predict the confines of the data nicely in each case. The small but consistent under-prediction of the experimental data by the CNW model can be explained by recognizing that the model assumes a completely non-wetting droplet when, in reality, only partial non-wetting is actually achieved. Finally, for micro-grooved surfaces this model represents an improvement over water retention models currently found in the literature. For this reason, it is useful not only for the prediction of the critical droplet size but also for the design of future micro-structured surfaces.

A sensitivity analysis was performed for the input parameters θ_{adv} and θ_{max} by changing their values $\pm 4^\circ$ to represent the experimental uncertainty of these measured variables and then examining the effect on the model prediction. These results, which

can be found in Fig. 14, reveal that the model is more sensitive to the specified value of θ_{\max} than θ_{adv} for non-wetting droplets, but overall the model was rather insensitive to small changes in both of these two input parameters. This indicates an overall robustness of the model and an ability to apply it even when an appreciable amount of experimental uncertainty exists for these input variables. The resulting model is useful for the prediction of the critical droplet size for sliding of composite droplets on micro-grooved aluminum surfaces where the channels are aligned parallel to gravity.

4. Conclusions

Water droplets placed on a micro-grooved aluminum surface using a micro-syringe exhibited significantly increased apparent contact angles, and the droplet volume at incipient sliding was reduced by more than 50% compared to droplets on a surface without micro-grooves. No chemical surface treatment was necessary to achieve this water repellency; it was accomplished primarily through the anisotropic surface topography. The droplet geometry shows an elongated base contour relative to a surface without micro-grooves, and discontinuities in the three-phase contact line are also introduced by the grooves. A mechanistic model is presented for predicting the critical droplet size on micro-grooved surfaces. This model extends earlier work by accounting for the droplet geometry and contact-line changes caused by the micro-grooves. The model is validated through comparisons of predicted to measured critical droplet sizes. The micro-structured surfaces introduced in this work are proposed for use in air-cooling and dehumidifying applications, but they may have other appli-

cations where the management of liquids on a surface is important.

Acknowledgment

We are grateful for financial support from the Air Conditioning and Refrigeration Center (ACRC) at the University of Illinois.

References

- [1] B.J. Briscoe, K.P. Galvin, *Colloids Surf.* 52 (1991) 219–229.
- [2] C.W. Extrand, A.N. Gent, *J. Colloid Interface Sci.* 138 (1990) 431–442.
- [3] R.A. Brown, F.M. Orr, L.E. Scriven, *J. Colloid Interface Sci.* 73 (1980) 76–87.
- [4] F. Milinazzo, M. Shinbrot, *J. Colloid Interface Sci.* 121 (1988) 254–264.
- [5] Y. Rotenberg, L. Boruvka, A.W. Neumann, *J. Colloid Interface Sci.* 102 (1984) 424–434.
- [6] C.W. Extrand, *Langmuir* 20 (2004) 5013–5018.
- [7] J.F. Oliver, C. Huh, S.G. Mason, *J. Adhesion* 8 (1977) 223–234.
- [8] M. Morita, T. Koga, H. Otsuka, A. Takahara, *Langmuir* 21 (2005) 911–918.
- [9] Z. Yoshimitsu, A. Nakajima, T. Watanabe, K. Hashimoto, *Langmuir* 18 (2002) 5818–5822.
- [10] Y. Chen, B. He, J. Lee, N.A. Patankar, *J. Colloid Interface Sci.* 281 (2005) 458–464.
- [11] C.W. Extrand, Y. Kumagai, *J. Colloid Interface Sci.* 170 (1995) 515–521.
- [12] P. Dimitrakopoulos, J.J.L. Higdon, *J. Fluid Mech.* 395 (1999) 181–209.
- [13] A.I. El Sherbini, A.M. Jacobi, *J. Colloid Interface Sci.* 273 (2004) 556–565.
- [14] A.I. El Sherbini, A.M. Jacobi, *J. Colloid Interface Sci.* 273 (2004) 566–575.
- [15] M. Bouteau, S. Cantin, F. Benhabib, F. Perrot, *J. Colloid Interface Sci.* 317 (2008) 247–254.
- [16] A.D. Sommers, A.M. Jacobi, *J. Micromech. Microeng.* 16 (8) (2006) 1571–1578.
- [17] P. Letellier, A. Mayaffre, M. Turmine, *J. Colloid Interface Sci.* 314 (2007) 604–614.
- [18] P.S. Yadav, P. Bahadur, R. Tadmor, K. Chaurasia, A. Leh, *Langmuir* 24 (2008) 3181–3184.